

REVIEW

Quantum beam diffraction measurement and topological analysis of tetrahedrally coordinated non-crystalline materials

Shinji Kohara^{1,†}, Koji Kimura^{1,2}, Motoki Shiga^{1,3,4,5}, Yohei Onodera¹,
Akihiko Hirata^{1,6,7,8} and Koichi Hayashi²

¹Center for Basic Research on Materials, National Institute for Materials Science, Tsukuba, Ibaraki 305–0047, Japan

²Department of Physical Science and Engineering, Nagoya Institute of Technology, Nagoya 466–8555, Japan

³Unprecedented-scale Data Analytics Center, Tohoku University, Sendai 980–8578, Japan

⁴Graduate School of Information Science, Tohoku University, Sendai 980–8579, Japan

⁵RIKEN Center for Advanced Intelligence Project, Tokyo 103–0027, Japan

⁶Department of Applied Mathematics/Department of Materials Science, Waseda University, Tokyo 169–8555, Japan

⁷Kagami Memorial Research Institute for Materials Science and Technology, Waseda University, Tokyo 169–0051, Japan

⁸WPI Advanced Institute for Materials Research, Tohoku University, Sendai 980–8577, Japan

The construction of large quantum beam facilities such as the synchrotron radiation facility SPring-8 and the high-intensity proton accelerator facility J-PARC has provided access to high-intensity, high-energy quantum beams that are essential for structural analyses of non-crystalline materials via diffraction measurements in Japan. The developments of quantum beam diffraction techniques led to significant advancements in the research field. By the complementary use of X-rays, which are sensitive to heavy elements, and neutrons, which are sensitive to light elements, along with the advances in computer simulations and topological analysis techniques, we have achieved a deep understanding of disordered structures with intermediate-range ordering. In this article, we review the recent results obtained by the complementary use of quantum beam diffraction and topological analyses of silica polymorphs, covering silica crystals and densified silica glasses. The comparison between the persistent homology analysis data and the ring size distribution has led to the classification of a series of densified silica glasses and crystals in terms of ring persistency (ring shape) and ring entropy (topological order–disorder). This is a new concept to understand the nature of order–disorder observed in a series of silica polymorphs without using diffraction data. We also discuss the differences among disordered materials, which comprises an AA₄ (A = Si) tetrahedral network (amorphous silicon), an AX₄ (A = Si, X = O) tetrahedral network (glassy silica), and a non-tetrahedral network due to isolated AX₄ (A = C, X = Cl) tetrahedra (liquid carbon tetrachloride) in terms of the origin of a three-peak structure, FSDP (Q_1), PP (Q_2), and Q_3 .

Key-words : Non-crystalline materials, Structure, X-ray diffraction, Neutron diffraction, Topology

[Received September 13, 2025; Accepted October 19, 2025]

1. Introduction

Non-crystalline materials such as glass, liquids, and amorphous materials lack the structural order found in crystalline phases, which results in broad ‘halo patterns’ in quantum beam diffraction data. Since non-crystalline materials lack structural descriptors such as lattice constants or space groups used in crystalline phases, it is impossible to determine atomic positions solely from diffraction data. Instead, the function best suited for describing the disordered structure of amorphous materials is the pair distribution function (PDF) $g(r)$.¹⁾ $g(r)$ represents the probability of finding another atom at the distance r from a

single atom located at the origin. $g(r)$ is obtained by a Fourier transform of the normalized quantum beam diffraction data, the Faber–Ziman²⁾ total structure factor $S(Q)$.

$$g(r) = 1 + \frac{1}{2\pi^2 r \rho} \int_{Q_{\min}}^{Q_{\max}} Q[S(Q) - 1] \sin(Qr) M(Q) dQ \quad (1)$$

Here, ρ represents the atomic number density, which is the number of atoms per unit volume. $Q = [(4\pi/\lambda) \sin \theta]$, where 2θ is the scattering angle and λ is the wavelength of the incident X-rays or neutrons] represents the magnitude of the scattering vector. $M(Q)$ is a modification function introduced to reduce the ripples caused by the truncation error of $S(Q)$ in a finite Q range in the Fourier transform of $S(Q)$, for which the Lorch function³⁾ has been used. However, since diffraction data over a wide Q range can now be measured with sufficient statistics, truncation

[†] Corresponding author: S. Kohara; E-mail: KOHARA.Shinji@nims.go.jp

[‡] Preface for this article: DOI <https://doi.org/10.2109/jcersj2.134.P4-1>

errors have been significantly reduced. Additionally, using such functions can lead to a decrease in real-space resolution, so there are many reports where $M(Q)$ is not introduced. However, the X-ray atomic form factor, which represents the scattering capability of atoms, depends on Q . Therefore, in multicomponent systems where the difference in atomic number between constituent atoms is large, it is often necessary to introduce $M(Q)$ to suppress the truncation error of the Q -dependent atomic form factor. Regarding $M(Q)$, new functions have been proposed,⁴⁾ and the effect of $M(Q)$ has been carefully discussed.⁵⁾ The relationships among the pair distribution function $g(r)$, the reduced pair distribution function $G(r)$, the total correlation function $T(r)$, and the radial distribution function $RDF(r)$ are expressed as follows.

$$g(r) = \frac{G(r)}{4\pi r\rho} + 1 \quad (2)$$

$$T(r) = G(r) + 4\pi r\rho = 4\pi r\rho g(r) \quad (3)$$

$$RDF(r) = rG(r) + 4\pi r\rho = rT(r) \quad (4)$$

To obtain the reliable real-space function with high resolution, it is necessary to measure diffraction patterns up to high Q , since the real-space resolution is determined by Q_{\max} in Eq. (1).⁶⁾ Large quantum beam facilities such as the synchrotron radiation facility SPring-8 and the high-intensity proton accelerator facility J-PARC have provided access to high-intensity, high-energy quantum beams that are essential for structural analyses of non-crystalline materials via diffraction measurements with high- Q data.

We previously have reviewed combined quantum beam diffraction measurements and computer simulations,^{7,8)} several studies on oxide glasses and high-temperature oxide melts,^{9,10)} and the topology in silica polymorphs.¹¹⁾ In this article, we review our recent studies on non-crystalline materials by diffraction measurements and a series of topological analysis techniques such as ring size, homology, ring shape, and tetrahedral order analyses. In particular, we introduce the concept of ‘ring entropy’ to understand the effects of ring shape and ring size distribution to the intermediate-range structure in silica polymorphs. Moreover, the origins of diffraction peaks in tetrahedrally coordinated non-crystalline materials are discussed.

2. X-ray and neutron diffraction data of silica (SiO₂) glass

Silica is the most important material that can form glass as a single component. The short-range ordering of this glass is the same as that of crystals consisting of SiO₄ tetrahedra with oxygen atoms sharing at the corner, forming a network structure. The structure factor $S(Q)$ of silica glass obtained from X-ray diffraction (SPring-8) and neutron diffraction (J-PARC) data is shown in **Fig. 1(a)**. When the glass is composed of n types ($n \geq 2$) or more of atoms, the X-ray total structure factor $S(Q)$ is the weighted sum of the partial structure factor $S_{ij}(Q)$ values corresponding to the correlations between atoms of the same or different types.

$$S^X(Q) = \sum_{i=1}^n \sum_{j=1}^n W_{ij}(Q) S_{ij}(Q) \quad (5)$$

$$\langle f(Q) \rangle^2 = \left(\sum_{i=1}^n c_i f_i(Q) \right)^2 \quad (6)$$

Here, c_i and $f_i(Q)$ are the molar fraction and atomic scattering factor of atom i , respectively, and $W_{ij}(Q)$ is the weighting factor defined by c_i and $f_i(Q)$, $W_{ij}(Q) = c_i c_j f_i(Q) f_j(Q) / \langle f(Q) \rangle^2$. In the case of silica glass,

$$\begin{aligned} S_{\text{SiO}_2}(Q) &= W_{\text{Si-Si}}(Q) S_{\text{Si-Si}}(Q) \\ &\quad + 2W_{\text{Si-O}}(Q) S_{\text{Si-O}}(Q) \\ &\quad + W_{\text{O-O}}(Q) S_{\text{O-O}}(Q) \end{aligned} \quad (7)$$

When $f_i(Q)$ is replaced with the atomic number, i.e., $f_i(Q=0)$, the relationships of the X-ray structure factor $S^X(Q)$ and the neutron structure factor $S^N(Q)$ obtained by replacing $f_i(Q)$ with the neutron scattering length b_i with the partial structure factor are expressed as follows.

$$\begin{aligned} S^X(Q) &= 0.218 S_{\text{Si-Si}}(Q) + 0.498 S_{\text{Si-O}}(Q) \\ &\quad + 0.284 S_{\text{O-O}}(Q) \end{aligned} \quad (8)$$

$$\begin{aligned} S^N(Q) &= 0.069 S_{\text{Si-Si}}(Q) + 0.388 S_{\text{Si-O}}(Q) \\ &\quad + 0.543 S_{\text{O-O}}(Q) \end{aligned} \quad (9)$$

X-rays are more sensitive to heavy elements, whereas neutrons are more sensitive to light elements. This difference in sensitivity is reflected in the different weights assigned to each $S_{ij}(Q)$. In fact, this difference in weight is manifested as the difference in $S(Q)$ in **Fig. 1(a)**.¹²⁾ The first sharp diffraction peak (FSDP, Q_1)^{13,14)} is observed at $Q \sim 1.5 \text{ \AA}^{-1}$ in $S^{X,N}(Q)$. This FSDP is considered a signature of the intermediate-range ordering in glass, and its peak position ($2\pi/Q_1$) and half-width ($2\pi/\Delta Q_1$) are estimated to have a periodicity of 4 Å and a coherence length of 10 Å, respectively.¹⁵⁾

$S^N(Q)$ shows a principal peak (PP, Q_2)¹⁴⁾ at $Q \sim 3 \text{ \AA}^{-1}$, but no such peak is observed in $S^X(Q)$, suggesting that PP reflects the oxygen–oxygen correlation. The $S_{ij}(Q)$ ^{15,16)} of silica glass derived from MD-RMC modelling is shown in **Fig. 1(a)**. It can be seen that $S_{\text{Si-Si}}(Q)$ and $S_{\text{O-O}}(Q)$ show positive peaks at $Q_2 \sim 3 \text{ \AA}^{-1}$, whereas $S_{\text{Si-O}}(Q)$ shows a negative peak. Since these positive and negative peaks are weighted by $W_{ij}(Q)$ in Eqs. (8) and (9), a large $W_{\text{O-O}}$ ($= 0.543$) results in a positive PP in $S^N(Q)$. However, in $S^X(Q)$, a large $W_{\text{Si-O}}$ ($= 0.498$) causes a negative PP. The origin of the negative peak at $Q \sim 3 \text{ \AA}^{-1}$ in $S_{\text{Si-O}}(Q)$ is discussed in Ref. 17).

The peak Q_3 observed at $Q \sim 5 \text{ \AA}^{-1}$ in $S^{X,N}(Q)$ reflects the nearest-neighbour correlation.¹⁸⁾ Onodera et al. applied RMC modelling to liquid mercury and confirmed its validity,¹⁵⁾ but further investigation is addressed in section 6 of this paper. **Figure 1(b)** shows the total correlation function $T^{X,N}(r)$ of silica glass¹²⁾ obtained by a Fourier transform of $S(Q)$. A peak corresponding to Si–O correlations is observed at 1.6 Å. The calculation of the peak area yields a coordination number of 4, confirming the formation of SiO₄ tetrahedra. An oxygen–oxygen correlation peak is observed at 2.6 Å, but since neutrons are more sensitive to oxygen atoms than X-rays, the peak is higher in neutron diffraction data. On the other hand, a peak corresponding

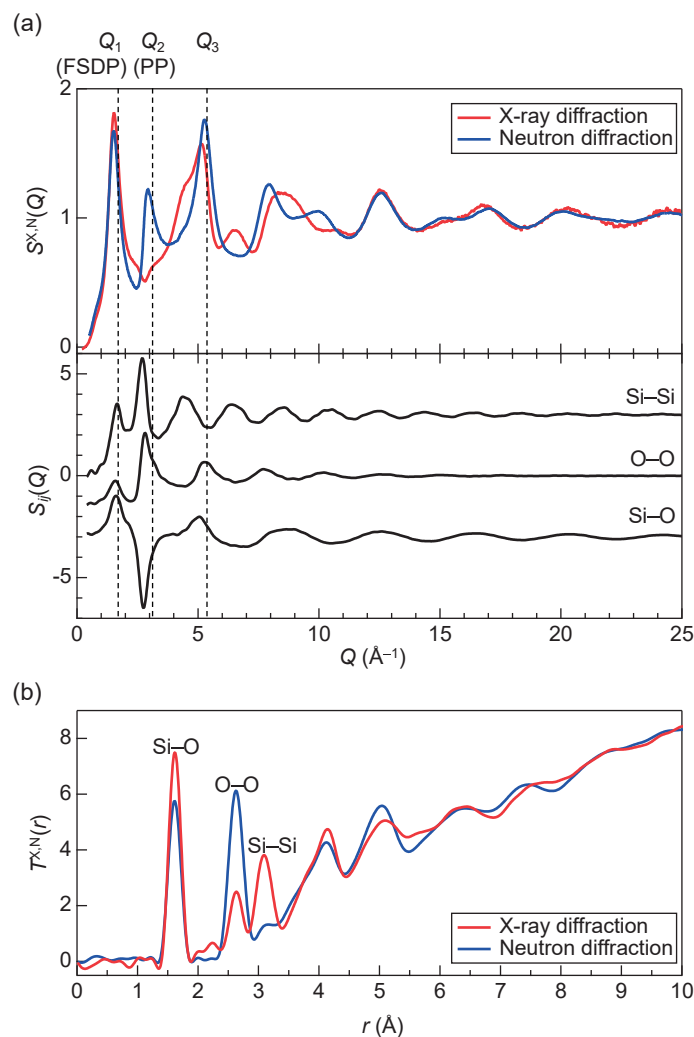


Fig. 1. (a) X-ray and neutron structure factors $S^{X,N}(Q)^{12)}$ together with Faber–Ziman partial structure factors $S_{ij}(Q)$ obtained from MD-RMC model.^{15,16)} (b) X-ray and neutron total correlation functions $T^{X,N}(r)$.¹²⁾

to silicon–silicon correlations is observed at 3.1 \AA , but the peak is higher in the diffraction data of X-rays, which are more sensitive to heavy elements. Thus, even in simple oxide glasses such as silica glass, the difference between X-ray and neutron diffraction data is clear.

3. Structure of silica crystal and glass

The short-range ordering of silica crystals (cristobalite, tridymite, quartz, and coesite) and glass consists of SiO_4 tetrahedra, which are interconnected by corner-sharing oxygen atoms to form a continuous network structure. In crystalline silica, Si atoms are surrounded by four Si atoms via O atoms and O atoms are surrounded by six O atoms via Si atoms (see Fig. 2). Figure 3 shows the distributions of the numbers of Si atoms around Si atom (a) and of O atoms around O atom (b) in silica glass obtained by MD-RMD modelling based on X-ray and neutron diffraction data.¹⁵⁾ The number of Si atoms around Si atom is almost 4, but only 70 % O atoms are surrounded by six O atoms in silica glass. This is an important structural feature in silica glass induced by disorder. Cooper proposed the topological disorder in silica glass on the basis of ring size

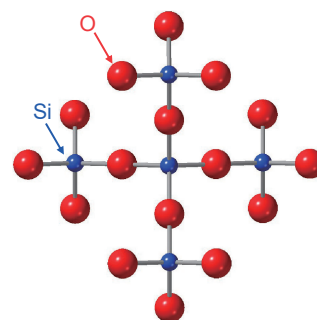


Fig. 2. Atomic configuration of β -cristobalite.

distribution, because silica glass shows a various-ring-size distribution.¹⁹⁾ Onodera et al. reported that cristobalite and tridymite have only sixfold rings (consisting of six SiO_4 tetrahedra), whereas quartz has a large fraction of eightfold rings in addition to sixfold rings. Coesite has a various-ring-size distribution similarly to silica glass, suggesting that coesite is topologically disordered. This feature is related to the broad neutron inelastic scattering spectrum of coesite, which is very similar to that of silica glass.²⁰⁾

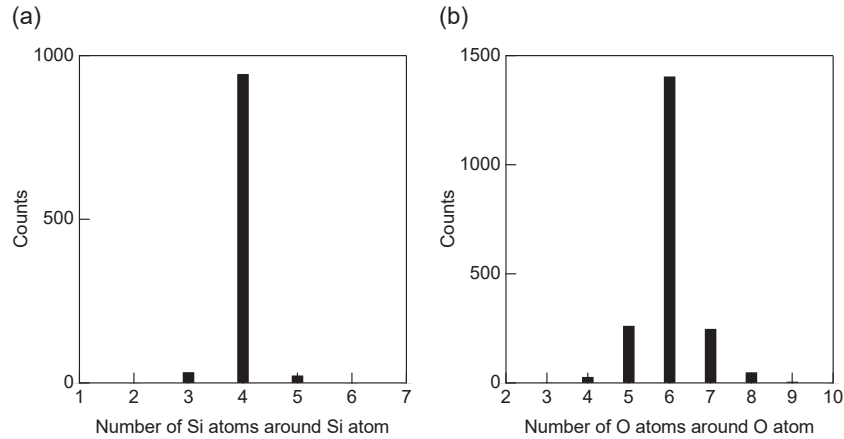


Fig. 3. (a) Number of silicon atoms around silicon atom and (b) that of oxygen atoms around oxygen atom obtained from MD-RMC model.

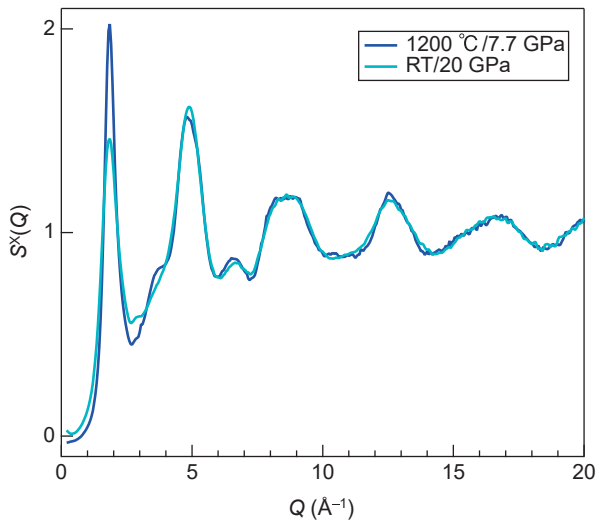


Fig. 4. X-ray total structure factors $S^X(Q)$ of two densified silica glasses.²⁰⁾

4. Structure and topology of densified silica glass

The structure of silica glass has been widely studied from ambient conditions^{1,6–12,15,16,21,22)} to high-pressure^{12,16,17,20–27)} and high-temperature^{12,17,20,21,28,30)} conditions by X-ray and neutron diffraction measurements. We have recently synthesized two silica glasses with the same density (2.7 g cm^{-3}) but different structures by hot and cold densifications.²⁰⁾ Figure 4 shows the X-ray total structure factors $S^X(Q)$ of silica glasses synthesized at $1200^\circ\text{C}/7.7 \text{ GPa}$ (hot densified glass, HDG) and $\text{RT}/20 \text{ GPa}$ (cold densified glass, CDG). The height of FSDP is maximum in HDG and minimum in CDG, suggesting that HDG is the most ordered glass and CDG is the most disordered glass. Moreover, we confirmed that CDG is not a permanently densified glass and its density decreases to 2.21 g cm^{-3} after heat treatment at 900°C .

We applied topological analysis techniques to a series of densified silica glasses to understand the intermediate-

range ordering. The combined use of ring size distribution analysis^{29,30)} and persistent homology analysis^{31–33)} is very useful for understanding the topology of densified silica glass.²⁰⁾ Figure 5(a) shows the persistence p_n [see Ref. 34)] of Si cycles in α -cristobalite,³⁵⁾ β -cristobalite,³⁶⁾ α -quartz,³⁷⁾ coesite,³⁸⁾ and a series of densified silica glasses calculated using a combination of the R.I.N.G.S. code,^{29,30)} SOVA,³⁹⁾ and HomCloud.³³⁾ It is found that the shape of a large ring changes with increasing density and the p_n of HDG is the smallest. This behaviour is in line with the change in the height of FSDP (Fig. S1). Intriguingly, the p_n values of the sixfold and eightfold rings in HDG are comparable to those of quartz, whose density is identical to that of HDG. It is also found that an unusually large p_n is observed for the eightfold rings in coesite. Although the fraction of eightfold rings is small, such symmetrical eightfold rings [see Fig. 5(b)] are observed in coesite, whose density is the highest in a series of tetrahedral corner-sharing silica.

Recently, we have reported that inter-tetrahedral oxygen–oxygen correlation is observed in silica glass, coesite, and siliceous zeolite MFI. Figure 6 shows the typical triangle O–O–O correlation³²⁾ extracted from O-centric persistence diagrams (PDs) for HDG and coesite, in which inter-tetrahedral O–O correlations (green sticks) are observed. This correlation is the origin of the sharp PP in neutron diffraction data for silica glass under high pressure.²⁴⁾

5. Topological analysis of Si–O rings

We propose a new analysis method to understand the ring statistics in silica polymorphs. To quantify the breadth of the ring size distribution, we define the ring entropy H as

$$H = - \sum_n F_n \ln(F_n), \quad (10)$$

where F_n denotes the fraction of Si–O rings with n -fold number of atoms in the primitive ring size distribution of each SiO_2 glass or crystal. H is zero when all rings have the same size, and it increases as the ring size distribution becomes broader. Thus, H provides a useful measure of the

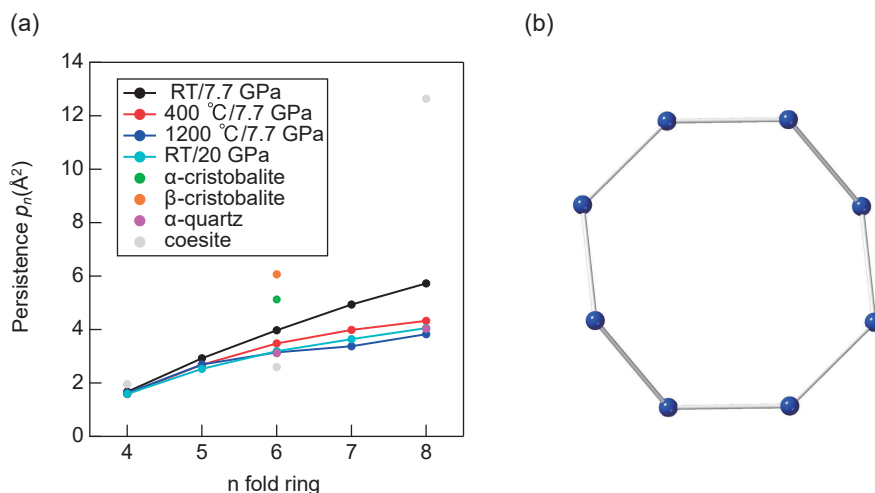


Fig. 5. (a) Ring persistence p_n of a series of silica crystals and densified silica glasses. (b) Highly symmetrical eightfold Si-Si cycle observed in coesite.

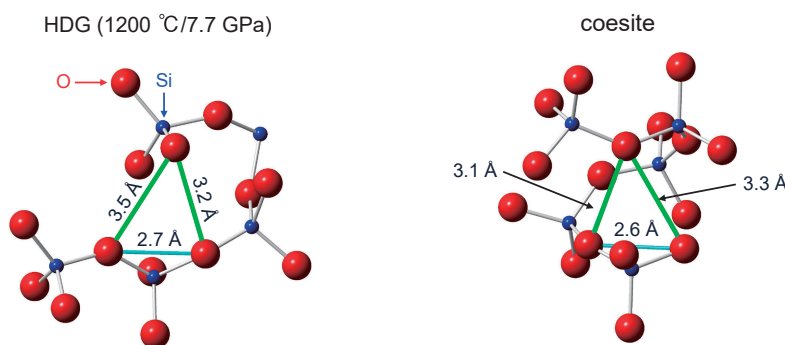


Fig. 6. Inter-tetrahedral oxygen–oxygen correlations up to 3.5 Å derived from persistent homology analysis of O-centric PDs. Intra- and inter-tetrahedral O–O correlations are indicated by cyan sticks and green sticks, respectively.

breadth of the ring size distribution. As mentioned in section 3, the concept of a topologically disordered network was proposed in Refs. 19) and 40) on the basis of ring size distribution. As a follow-up, here we introduce the ring entropy H , which enables the degree of topological disorder to be characterized quantitatively.

We also define the average persistence of the Si cycles, A , as

$$A = \sum_n F_n \frac{p_n}{n}, \quad (11)$$

where p_n is the persistence of the n -fold Si cycles defined by d_k-b_k derived by persistent homology analysis.^{31–33)} A characterizes the overall degree of symmetry of the rings in each SiO_2 compound. Smaller and larger A values correspond to more distorted and more symmetrical ring shapes, respectively.

Figure 7 shows a two-dimensional plot of A versus H for a series of silica polymorphs. Because both α - and β -cristobalites consist only of sixfold rings,²⁰⁾ their H values are zero. On the other hand, the ring shapes in β -cristobalite are more symmetric than those in α -cristobalite,²⁰⁾ and therefore, β -cristobalite exhibits a larger A value than α -cristobalite. Unlike cristobalite, α -quartz contains

rings of two different sizes, as determined from the primitive criterion,²⁰⁾ i.e., six- and eightfold rings. As a result, α -quartz shows a finite H value of 0.45. In addition, α -quartz exhibits a smaller A value than cristobalite, which reasonably reflects the more distorted ring shapes in α -quartz than in cristobalite.²⁰⁾

Compared with these crystals, the H values of SiO_2 glasses are larger because of the broader ring size distribution of the glasses than of cristobalite and quartz.²⁰⁾ A decreases in the following order of the glass samples synthesized under different conditions: RT/7.7 GPa, 400 °C/7.7 GPa, RT/20 GPa, and 1200 °C/7.7 GPa. This trend is well correlated with the increase in density.²⁰⁾ This correlation is further supported by the fact that the glasses synthesized at RT/20 GPa and 1200 °C/7.7 GPa exhibit both similar densities²⁰⁾ and A values. These results indicate that the densification of SiO_2 glasses induces the distortion of constituent rings.

Note that coesite data points cluster the SiO_2 glasses in Fig. 7. In particular, the similarity in H values between coesite and SiO_2 glasses suggests a similar degree of topological disorder. This similarity may be related to a broad peak observed in the inelastic neutron scattering data for

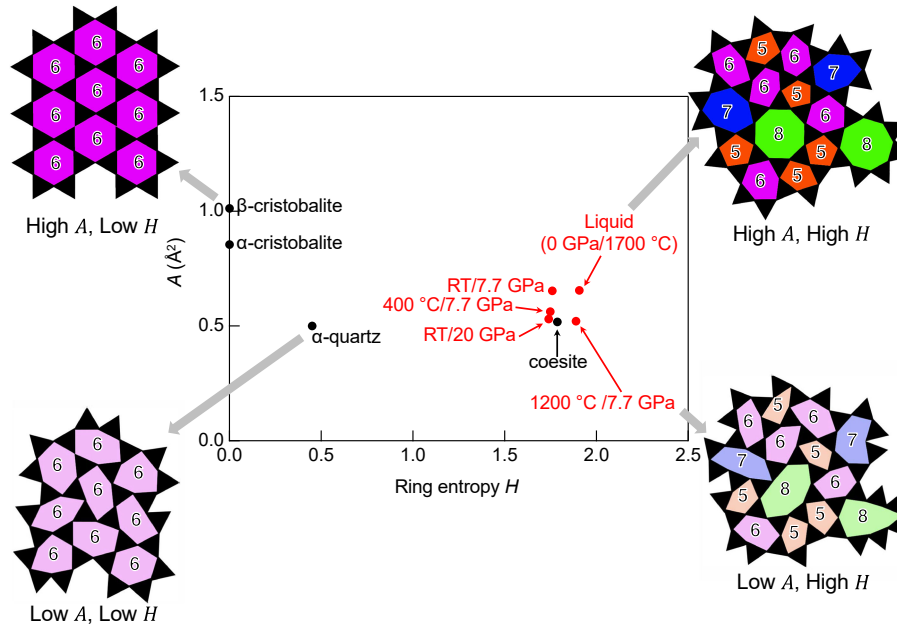


Fig. 7. Two-dimensional plot of A versus H for a series of silica polymorphs.

coesite,²⁰⁾ which is very similar to the feature of the boson peak observed in SiO_2 glasses as mentioned in section 3.

Although the H and A values of liquid silica are identical to those of silica glass, they are larger, indicating that silica in the liquid state is topologically more disordered than that in the glassy state,⁴¹⁾ whereas its rings are overall less distorted.

On the basis of the above discussion, we schematically illustrate two-dimensional corner-sharing networks for different combinations of A and H values in Fig. 7. For low A and high H , the network consists of rings with uniform size and symmetric shapes (upper left in Fig. 7), which corresponds to β -cristobalite. As H increases, a wide variety of ring sizes appear, whereas the rings generally maintain their symmetric shapes (upper right in Fig. 7). In contrast, as A decreases, the rings become distorted, while the network still consists of rings with the same size (lower left in Fig. 7). When A is low and H is high, the network is composed of distorted rings with different sizes (lower right in Fig. 7).

It is worth mentioning that both A and H are insensitive to the distinction between crystalline and non-crystalline states. In fact, both the crystals and glasses can exhibit similar values of A and H as shown in Fig. 7 for SiO_2 glasses and coesite. Therefore, A and H provide a unified framework for evaluating topological features across both crystalline and non-crystalline materials. In addition, the ring entropy H represents different measure of order and disorder from that inferred from the FSDP. Figure S1 presents the $S(Q)$ in the low- Q region for SiO_2 glasses synthesized at various temperatures and under a pressure of 7.7 GPa. Compared with the $S(Q)$ of the glass synthesized at RT/7.7 GPa, which is almost identical to that of the pristine glass in terms of the position/height of FSDP and density, the sample prepared at 400 °C/7.7 GPa exhib-

its an FSDP with reduced height and a shift to a higher- Q region. As the temperature further increases, the height of the FSDP is significantly increased, reaching its maximum at 1200 °C/7.7 GPa, indicating that the hot-densified glass synthesized at this condition is the most ordered glass, as discussed in section 4. On the other hand, this hot-densified glass shows the highest H value among the glasses synthesized under different temperatures at 7.7 GPa, as shown in Fig. 7, suggesting the strong topological disorder of the glass synthesized at 1200 °C/7.7 GPa. These results highlight the conceptual difference between topological order/disorder proposed by Cooper and Gupta and that proposed in this section.

6. Understanding the origin of Q_3 in non-crystalline materials

The origin of diffraction peaks of non-crystalline materials has been discussed for long time.^{11,13,15,18)} The length scale of intermediate-range order manifested by diffraction peaks in terms of peak position and peak width was discussed by Salmon and Zeidler in Ref. 42). Very recently, the ring size distribution in silica glass was deduced by the analysis of FSDP, which seems to be a challenging approach.⁴³⁾ Figure 8 shows atomic configurations of amorphous silicon,⁴¹⁾ glassy silica,¹⁵⁾ and liquid carbon tetrachloride.⁴⁴⁾ Amorphous Si has a perfect SiSi_4 tetrahedral network, whereas glassy silica has a SiO_4 tetrahedral network in which Si atom is fourfold and O atom is twofold. The short-range structure of liquid carbon tetrachloride is a CCl_4 tetrahedron, but CCl_4 tetrahedra are isolated. In our previous study, we confirmed that the Q_3 of liquid Hg can be reproduced by a random atomic configuration with a cut-off distance of 2.6 Å.¹⁵⁾ Here, we calculate the $S(Q)$ of a SiSi_4 tetrahedron (first and second Si-Si correlations), a SiO_4 tetrahedron (silicon-oxygen and

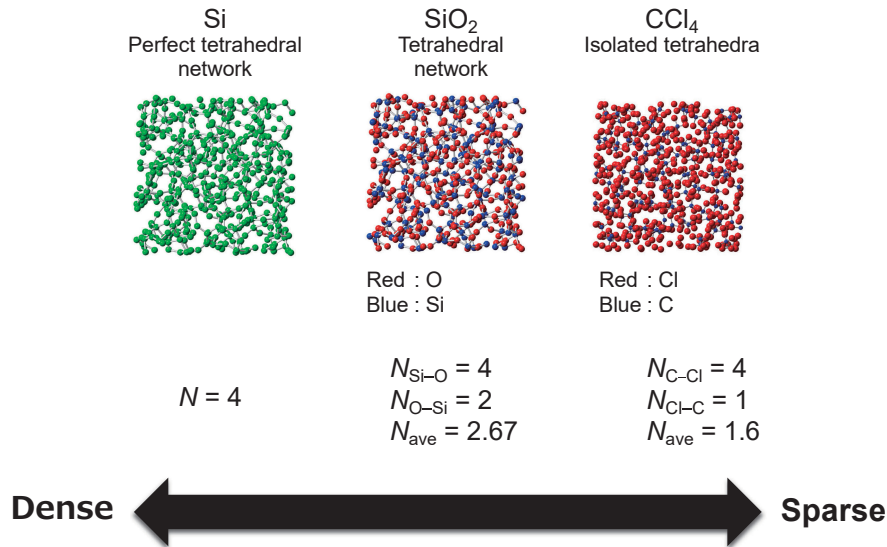


Fig. 8. Atomic configurations of amorphous silicon,⁴¹⁾ glassy silica,¹⁵⁾ and liquid carbon tetrachloride⁴⁴⁾ together with coordination numbers obtained by MD-RMC models for amorphous silicon and glassy silica, and RMC-MM model for liquid carbon tetrachloride.

oxygen–oxygen correlations), and a CCl₄ tetrahedron (carbon–chlorine and chlorine–chlorine correlations) using the following equations:^{45,46)}

$$S(Q) = \frac{c_i N_{ij} f_i(Q) f_j(Q)}{\langle f(Q) \rangle^2} \exp\left(-\frac{1}{2} l_{ij}^2 Q^2\right) \times \frac{\sin(\pi Q / Q_{\max})}{\pi Q / Q_{\max}} \frac{\sin(Q r_{ij})}{r_{ij}} \quad (12)$$

and

$$\langle f(Q) \rangle^2 = \left(\sum_i c_i f_i(Q) \right)^2, \quad (13)$$

where c_i and $f_i(Q)$ are the concentration and atomic form factor of i , respectively. r_{ij} is the atomic distance between i and j , N_{ij} is the coordination number of j around i , and l_{ij} is a convergence factor that represents the static and thermal disorders of the i – j correlation.

Figure 9 shows the X-ray total structure factor $S^X(Q)$ of amorphous Si,⁴⁷⁾ the neutron total structure factors $S^N(Q)$ of glassy silica¹²⁾ and liquid carbon tetrachloride,⁴⁸⁾ together with the $S^X(Q)$ of a SiSi₄ tetrahedron and the $S^N(Q)$ of a SiO₄ tetrahedron and a CCl₄ tetrahedron calculated using Eq. (12). It is confirmed that FSDP and PP cannot be reproduced by a tetrahedron for glassy silica. As can be seen in the figure, a CCl₄ model shows a single PP, but experimental data shows two peaks due to the orientational correlation^{49,50)} of CCl₄ molecules. The hard sphere Monte Carlo^{50,51)} model gives a single PP.⁵²⁾ Only the Q^3 of liquid carbon tetrachloride is reproduced by a CCl₄ tetrahedron probably owing to the non-tetrahedral network structure (CCl₄ molecules are isolated).

Here, we address more the origin of PP. The origin of FSDP has been widely discussed,^{11,13,15,18)} while the origin of PP can be understood in terms of inter-tetrahedral X–X correlation in AX₄ tetrahedrally coordinated system in this article. Since metallic glasses do not show an FSDP nor a

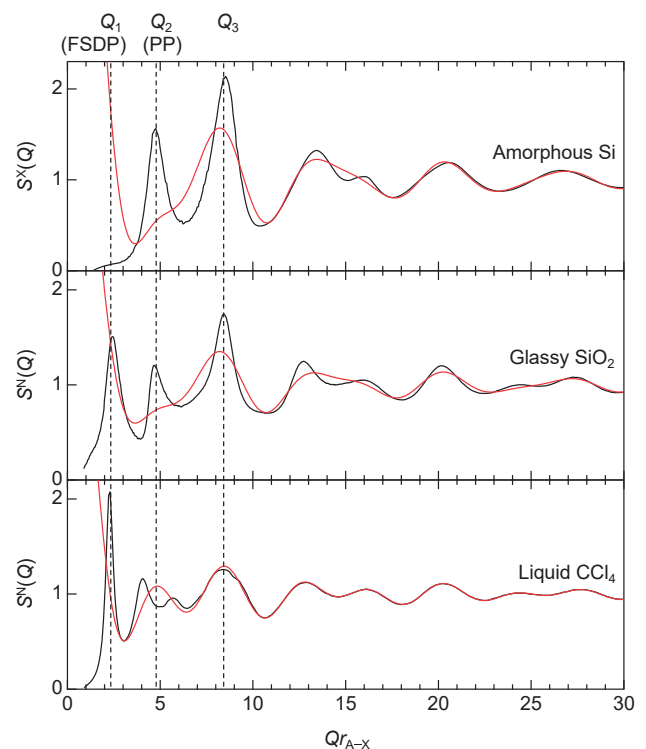


Fig. 9. X-ray total structure factors $S^X(Q)$ of amorphous silicon⁴⁷⁾ and neutron total structure factors $S^N(Q)$ of liquid carbon tetrachloride⁴⁸⁾ and glassy silica¹²⁾ together with $S^X(Q)$ of SiSi₄ and $S^N(Q)$ of SiO₄ and CCl₄ calculated using Eq. (12). The scattering vector Q is scaled by multiplying by r_{A-X} (distance between centre and corner of tetrahedron). Black curve; experimental data, red curve; calculated data.

PP,^{15,18)} we suggest that the origin of PP can be attributed to the correlation of the vertex of polyhedra in amorphous silicon and liquid carbon tetrachloride.

7. Conclusions

In this article, we review recent results obtained by the complementary use of quantum beam diffraction and topological analysis for silica polymorphs. First, we introduced the state-of-the-art X-ray and neutron diffraction data of silica glass measured at SPring-8 and J-PARC, respectively.

A combination of quantum beam diffraction measurements and computer simulations,^{7,8)} several studies on oxide glasses and high-temperature oxide melts,^{9,10)} and the topology in silica polymorphs¹¹⁾ have been reviewed in our previous articles. In the present article, we compare atomic arrangements in silica crystals and glass, with special focus on the number of silicon atoms around silicon atom, and that of oxygen atoms around oxygen atom. Moreover, we introduced a series of densified silica glasses synthesized by hot and cold densifications to understand the differences in diffraction data and ring persistency. The comparison between the persistent homology analysis data and the ring size distribution has led to the classification of a series of densified silica glasses and crystals in terms of ring persistency (ring shape) and ring entropy (topological order–disorder) without using diffraction data. This is a crucial new concept to understand the nature of order within disorder⁵³⁾ observed in a series of silica polymorphs.

Finally, we interpreted the diffraction peak in tetrahedrally coordinated non-crystalline materials. As a result, we found differences among amorphous silicon, glassy silica, and liquid carbon tetrachloride in terms of the origins of a three-peak structure, FSDP (Q_1), PP (Q_2), and Q_3 .

The understanding of diffraction peaks in non-crystalline materials is the first step toward understanding the nature of order within disorder. Moreover, the introduction of topological analysis enables us to directly compare between crystalline and non-crystalline materials, which does not depend on the presence or absence of the Bragg peak.

Acknowledgements This work was partially supported by JSPS Grants-in-Aid for Transformative Research Areas (A) “Hyper-Ordered Structures Science” (Grant Numbers 20H05878, 20H05881, and 20H05884). Discussions with Professor I. Obayashi and Dr. K. Nakashima are gratefully appreciated. MD simulations were performed using the Numerical Materials Simulator at the National Institute for Materials Science (NIMS).

References

- 1) K. A. Kirchner, D. R. Cassar, E. D. Zanotto, M. Ono, S. H. Kim, K. Doss, M. L. Bødker, M. M. Smedskjaer, S. Kohara, L. Tang, M. Bauchy, C. J. Wilkinson, Y. Yang, R. S. Welch, M. Mancini and J. C. Mauro, *Chem. Rev.* **123**, 1774 (2023).
- 2) T. E. Faber and J. M. Ziman, *Philos. Mag.* **11**, 153 (1965).
- 3) E. Lorch, *J. Phys. C Solid State* **2**, 229 (1969).
- 4) A. K. Soper and E. R. Barney, *J. Appl. Crystallogr.* **44**, 714 (2011).
- 5) J. E. Proctor, C. G. Pruteanu, B. Moss, M. A. Kuzovnikov, G. J. Ackland, C. W. Monk and S. Anzellini, *J. Appl. Phys.* **134**, 114701 (2023).
- 6) S. Kohara, K. Ohara, H. Tajiri, C. Song, O. Sakata, T. Usuki, Y. Benino, A. Mizuno, A. Masuno, J. T. Okada, T. Ishikawa and S. Hosokawa, *Z. Phys. Chem.* **230**, 339 (2016).
- 7) S. Kohara and P. S. Salmon, *Adv. Phys.: X* **1**, 640 (2016).
- 8) S. Kohara, *J. Ceram. Soc. Jpn.* **125**, 799 (2017).
- 9) S. Kohara, *J. Ceram. Soc. Jpn.* **130**, 531 (2022).
- 10) Y. Onodera, *J. Ceram. Soc. Jpn.* **130**, 627 (2022).
- 11) S. Kohara, *J. Ceram. Soc. Jpn.* **133**, 488 (2025).
- 12) S. Sato, M. Miyakawa, T. Taniguchi, Y. Onodera, K. Ohara, K. Ikeda, N. Kitamura, Y. Idemoto and S. Kohara, *J. Ceram. Soc. Jpn.* **132**, 427 (2024).
- 13) D. L. Price, S. C. Moss, R. Reijers, M.-L. Saboungi and S. Susman, *J. Phys. C Solid State* **21**, L1069 (1988).
- 14) P. S. Salmon, R. A. Martin, P. E. Mason and G. J. Cuello, *Nature* **435**, 75 (2005).
- 15) Y. Onodera, S. Kohara, S. Tahara, A. Masuno, H. Inoue, M. Shiga, A. Hirata, K. Tsuchiya, Y. Hiraoka, I. Obayashi, K. Ohara, A. Mizuno and O. Sakata, *J. Ceram. Soc. Jpn.* **127**, 853 (2019).
- 16) K. Ohara, Y. Onodera, M. Murakami and S. Kohara, *J. Phys.-Condens. Mat.* **33**, 383001 (2021).
- 17) S. Hayafune, T. Sakamaki, H. Ichikawa, Y. Onodera, S. Kohara and A. Suzuki, *J. Ceram. Soc. Jpn.* **133**, 242 (2025).
- 18) P. S. Salmon and A. Zeidler, *J. Stat. Mech.-Theory E* **2019**, 114006 (2019).
- 19) A. R. Cooper, *Phys. Chem. Glasses* **19**, 60 (1978).
- 20) Y. Onodera, S. Kohara, P. S. Salmon, A. Hirata, N. Nishiyama, S. Kitani, A. Zeidler, M. Shiga, A. Masuno, H. Inoue, S. Tahara, A. Polidori, H. E. Fischer, T. Mori, S. Kojima, H. Kawaji, A. I. Kolesnikov, M. B. Stone, M. G. Tucker, M. T. McDonnell, A. C. Hannon, Y. Hiraoka, I. Obayashi, T. Nakamura, J. Akola, Y. Fujii, K. Ohara, T. Taniguchi and O. Sakata, *NPG Asia Mater.* **12**, 85 (2020).
- 21) Y. Inamura, Y. Katayama, W. Utsumi and K. Funakoshi, *Phys. Rev. Lett.* **93**, 015501 (2004).
- 22) T. Sato and N. Funamori, *Phys. Rev. Lett.* **101**, 255502 (2008).
- 23) C. J. Benmore, E. Soignard, S. A. Amin, M. Guthrie, S. D. Shastri, P. L. Lee and J. L. Yarger, *Phys. Rev. B* **81**, 054105 (2010).
- 24) A. Zeidler, K. Wezka, R. F. Rowlands, D. A. J. Whittaker, P. S. Salmon, A. Polidori, J. W. E. Drewitt, S. Klotz, H. E. Fischer, M. C. Wilding, C. L. Bull, M. G. Tucker and M. Wilson, *Phys. Rev. Lett.* **113**, 135501 (2014).
- 25) M. Murakami, S. Kohara, N. Kitamura, J. Akola, H. Inoue, A. Hirata, Y. Hiraoka, Y. Onodera, I. Obayashi, J. Kalikka, N. Hirao, T. Musso, A. S. Foster, Y. Idemoto, O. Sakata and Y. Ohishi, *Phys. Rev. B* **99**, 045153 (2019).
- 26) Y. Kono, K. Ohara, N. M. Kondo, H. Yamada, S. Hiroi, F. Noritake, K. Nitta, O. Sekizawa, Y. Higo, Y. Tange, H. Yumoto, T. Koyama, H. Yamazaki, Y. Senba, H. Ohashi, S. Goto, I. Inoue, Y. Hayashi, K. Tamasaku, T. Osaka, J. Yamada and M. Yabashi, *Nat. Commun.* **13**, 2292 (2022).

- 27) M. Guerette, M. R. Ackerson, J. Thomas, F. Yuan, E. B. Watson, D. Walker and L. Huang, *Sci. Rep.-UK* 5, 15343 (2015).
- 28) Q. Mei, C. J. Benmore and J. K. R. Weber, *Phys. Rev. Lett.* 98, 057802 (2007).
- 29) S. L. Roux and P. Jund, *Comp. Mater. Sci.* 49, 70 (2010).
- 30) S. L. Roux and P. Jund, *Comp. Mater. Sci.* 50, 1217 (2011).
- 31) I. Obayashi, T. Nakamura and Y. Hiraoka, *J. Phys. Soc. Jpn.* 91, 091013 (2022).
- 32) Y. Hiraoka, T. Nakamura, A. Hirata, E. G. Escobar, K. Matsue and Y. Nishiura, *P. Natl. Acad. Sci. USA* 113, 7035 (2016).
- 33) I. Obayashi, HomCloud, <https://homcloud.dev/index.en.html>.
- 34) P. S. Salmon, A. Zeidler, M. Shiga, Y. Onodera and S. Kohara, *Phys. Rev. B* 107, 144203 (2023).
- 35) J. J. Pluth, J. V. Smith and J. Faber, *J. Appl. Phys.* 57, 1045 (1985).
- 36) R. W. G. Wyckoff, *Z. Krist.-Cryst. Mater.* 62, 189 (1926).
- 37) K. Kihara, *Eur. J. Mineral.* 2, 63 (1990).
- 38) L. Levien and C. T. Prewitt, *Am. Mineral.* 66, 324 (1981).
- 39) <https://www.shiga-lab.org/sova>.
- 40) P. K. Gupta, *J. Am. Ceram. Soc.* 76, 1088 (1993).
- 41) S. Kohara, M. Shiga, Y. Onodera, H. Masai, A. Hirata, M. Murakami, T. Morishita, K. Kimura and K. Hayashi, *Sci. Rep.-UK* 11, 22180 (2021).
- 42) P. S. Salmon and A. Zeidler, *Phys. Chem. Chem. Phys.* 15, 15286 (2013).
- 43) Q. Zhou, Y. Shi, B. Deng, J. Neuefeind and M. Bauchy, *Sci. Adv.* 7, eabh1761 (2021).
- 44) H. Morita, S. Kohara and T. Usuki, *J. Mol. Liq.* 147, 182 (2009).
- 45) R. L. Mozzi and B. E. Warren, *J. Appl. Crystallogr.* 2, 164 (1969).
- 46) Y. Onodera, Y. Takimoto, H. Hijiya, Q. Li, H. Tajiri, T. Ina and S. Kohara, *NPG Asia Mater.* 16, 22 (2024).
- 47) K. Laaziri, S. Kycia, S. Roorda, M. Chicoine, J. L. Robertson, J. Wang and S. C. Moss, *Phys. Rev. Lett.* 82, 3460 (1999).
- 48) Y. Onodera, private communication.
- 49) M. Misawa, *J. Chem. Phys.* 91, 5648 (1989).
- 50) Sz. Pothoczki, L. Temleitner and L. Pusztai, *Chem. Rev.* 115, 13308 (2015).
- 51) S. Kohara and L. Pusztai, in “Computer Simulations of Glasses: Methodologies and Applications”, Ed. by J. Du and A. N. Cormack, Wiley-American Ceramic Society, Hoboken (2022) pp. 60–88.
- 52) Sz. Pothoczki, L. Temleitner, P. J  v  ri, S. Kohara and L. Pusztai, *J. Chem. Phys.* 130, 064503 (2009).
- 53) P. S. Salmon, *Nat. Mater.* 1, 87 (2002).